Detection of Hypertensive Retinopathy Using Vessel Measurements and Textural Features

Carla Agurto-*IEEE Member*, Vinayak Joshi-*IEEE Member, Sheila Nemeth, Peter Soliz-IEEE Member, and* Simon Barriga-*IEEE Member*

***Abstract*- Features that indicate hypertensive retinopathy have been well described in the medical literature. This paper presents a new system to automatically classify subjects with hypertensive retinopathy (HR) using digital color fundus images. Our method consists of the following steps: 1) normalization and enhancement of the image; 2) determination of regions of interest based on automatic location of the optic disc; 3) segmentation of the retinal vasculature and measurement of vessel width and tortuosity; 4) extraction of color features; 5) classification of vessel segments as arteries or veins; 6) calculation of artery-vein ratios using the six widest (major) vessels for each category; 7) calculation of mean red intensity and saturation values for all arteries; 8) calculation of amplitude-modulation frequency-modulation (AM-FM) features for entire image; and 9) classification of features into HR and non-HR using linear regression. This approach was tested on 74 digital color fundus photographs taken with TOPCON and CANON retinal cameras using leave-one out cross validation. An area under the ROC curve (AUC) of 0.84 was achieved with sensitivity and specificity of 90% and 67%, respectively.**

I. Introduction

Diabetic retinopathy screening programs have found a significant incidence of other systemic conditions that present on the retina as vascular abnormalities, e.g. hypertensive retinopathy (HR). HR is the long-term damage to the retina due to high blood pressure that accumulates on the eye over a period of several years even with individuals who control their blood pressure with medication. Unfortunately, most of the cases are asymptomatic but can be identified through retinal imaging. Early vascular changes associated with HR include generalized retinal arteriolar narrowing, changes in the arteriolar junction (AV nicking), and changes in the arteriolar light reflex (copper wiring or silver wiring) [1]. In addition, increased retinal vessel tortuosity has been identified as a risk factor of coronary disease, particularly hypertension [2]. It is important to detect HR since studies have demonstrated that it is associated with an increased long-term risk for stroke [3].

In this work, we present a fully automatic method to detect HR based on classification of features that characterize HR such as AVR, silver/copper wiring, tortuosity and vessel abnormalities. This paper is organized as follows. Section II describes the data used to train and test the automatic detection of HR; Section III describes the methods implemented; Section IV describes the results obtained; Section V presents valuable points for discussion and summarizes our conclusions.

Research supported in part by NIH grants EY020015, R43EY024169

C. Agurto, V. Joshi, S. Nemeth, P. Soliz, and S. Barriga are with VisionQuest Biomedical, LLC, Albuquerque, NM, 87109; e-mail: cagurto@visionquest-bio.com

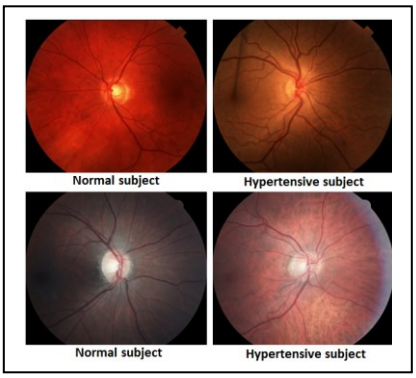

Figure 1. Sample images from our database. Top row: TOPCON . Bottom row Canon.

II. Data

We randomly selected 74 retinal vasculature marked images from VisionQuest's eye disease screening database to develop our methodology and evaluate its performance. Of these, 45 images are from normal subjects and do not show any sign of HR; 29 show signs of HR such as generalized and focal arteriole narrowing, AV nicking, silver or copper-wiring and tortuous arteries and veins. All images were of sufficient quality for clinical determination, as judged by a licensed optometrist. The images were captured using two cameras: TOPCON TRC 50EX and CANON CR-1 Mark II. All images have a 45-degree field of view (FOV) and are centered in the optic disc. The images were normalized to a standard size of 2224x1888 pixels, which is the smallest size among the set). Fig 1 shows sample images from HR and normal subjects.

III. Methods

The proposed automatic hypertension classification methodology consists of ten steps which are described next.

A. Pre-processing

Since some of the steps implemented for the detection of HR used color information, it is important to normalize the images before the extraction of features. Images are processed using a histogram stretching technique to achieve normalized entropy for all images. Based on the mean entropy value across all the images in the database, the target entropy values for the red, green, and blue channel were determined to be 7, 6.5 and 5.5 bits, respectively. We then perform color normalization using the mean intensity value with target values for the red,

978-1-4244-7929-0/14/$26.00 ©2014 IEEE

green, and blue channel of 100, 75 and 40, respectively. Fig 2 shows the result of this color normalization process.

B. Optic disc location and ROI selection

Accurate optic disc (OD) localization is necessary for determining the region of interest (ROI) to calculate the artery-vein ratio (AVR), tortuosity and other features. We use an automated and fast optic disc localization algorithm that was previously developed by our group [4]. After the coordinates of the optic disc are located, two regions of interest are selected based on findings of previous studies [5]. To determine AVR and silver/copper wiring, the vessel information within an annular region of 1 to 1.5 disc diameters away from the OD center is used. This ROI is referred to as region R1 (See Fig 3). Tortuosity and the textural features are calculated using the vessel information within an annular region of 1 to 2.5 disc diameters away from the OD center. This ROI is referred as R2 (see Fig. 3).

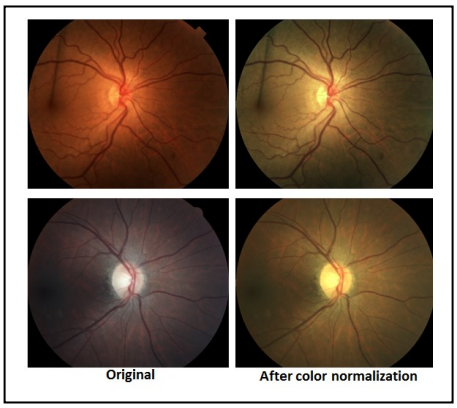

Figure 2. Examples of images after applying the color normalization. Left, original images; right, entropy and color normalized images.

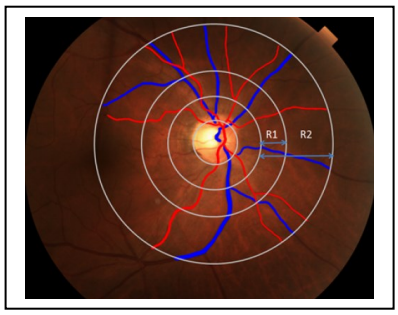

Figure 3. Regions of interest for HR detection. The vessels marked in blue and red represent the veins and arteries respectively.

C. Vessel segmentation

Accurate blood vessel segmentation is a preliminary and essential step in order to achieve vessel measurement such as width for AVR and tortuosity. The automated vessel segmentation method which is used, described in [6], is based on a multi-scale linear structure enhancement and the second order local entropy thresholding.

D. Vessel partition

A thinning algorithm [7] is applied to the segmented vessels to analyze the vascular network and to trim binary vessels until only single pixel-wide centerlines remain. Landmark points (vessel cross-overs and branch points) are detected by counting the number of neighbors for each centerline pixel, and the pixels which have three or more neighbors, are removed. This operation divides the vascular network into a collection of vessel segments which will be classified into arteries or veins and used for extraction of color and textural features for HR classification, as described in the following sections.

E. Artery-Vein feature extraction and classification

Multiple features are directly extracted from each vessel segment to classify it as an artery or vein. A total of 72 multi-scale color, contrast, and morphological features described in [8] are extracted from each vessel segment. These features characterize the visual difference between arteries and veins such as color, color variation, as well as the strength and size of the central reflex. Classification is performed using a regression classifier [8], which assigns "hard" labels of 'artery' or 'vein' for each of the vessel segments in region R1.

F. Artery-Vein ratio (AVR) calculation

After classifying arteries and veins, the six widest (major) veins and arteries from the processed vessel segments in each image are automatically selected. The width of the vessel is calculated by dividing it into small segments of 15 pixels and determining their length by measuring the perpendicular line that intersects the vessel edges. The final width for the segment is the median of all the widths obtained for the mini-segments. AVR is calculated using the width of the six widest arteries and veins and defined as the ratio of the Central Retinal Artery Equivalent (CRAE) and the Central Retinal Vein Equivalent (CRVE). Knudtson et al. [5] described an iterative process for pairing up vessels to calculate CRAE and CRVE. This is an iterative method that pairs the largest vessel with the smallest one until a single number is obtained. The following formulas are used for the calculation of each pair of vessels.

$$W_{arteries} = 0.88*(w_1+w_2)^{1/2}. \quad (1)$$

$$W_{venules} = 0.95*(w_1+w_2)^{1/2}. \quad (2)$$

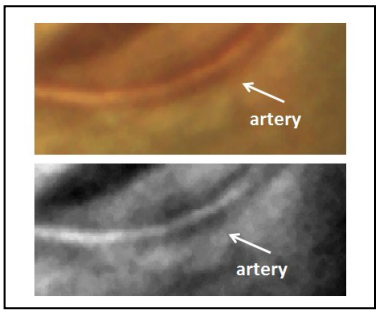

Figure 4. Example of an artery with copper wiring. Top: original, bottom: only red channel.

G. Silver/copper wiring

Copper/silver wiring is detected by characterizing the color of the vessels in the red and saturation channels. These two color channels capture the amount of light

reflex resulting from HR. Fig. 4 shows how the intensity value in the red channel increases in the center of the artery because of the copper wiring. From the mean values obtained for all of the artery segments in the image, we select the three largest values and the mean of these values is used to characterize each image.

H. Tortuosity index

Vessel tortuosity values are calculated using three different methods, which add robustness to the measurements. The first method to calculate the tortuosity index is the conventional measurement of the ratio of the arc length and the length of the segment. The second method described in [9] calculates the total curvature using a numerical differentiation method. Finally, the third method incorporates the values obtained with the first method, the magnitude of curvature of a vessel (Θ), and the number of curvature sign changes along the vessel course (n) [10]. The three measurements are obtained for individual sections of a vessel segment. Local tortuosity contributions are joined to obtain a tortuosity index (TI) per vessel segment using the formula in Eq. 3. In order to obtain a global tortuosity index for each image, the mean of 5 highest TI values is used to characterize each image. A total of three tortuosity features per image for the classifier are obtained.

$$TI = \frac{[n+1]*\sum_{i=1}^{m}[\theta i]*\sum_{i=1}^{m}[(Lci/Lxi)]}{Lc*m*m} \quad (3)$$

I. Textural features

In previous publication [11], we showed that the features obtained with amplitude-modulation frequency-modulation (AM-FM) captured relevant information of retinal vascular features. Here these features are included in order to add information about the retinal vasculature. Information on seven statistical measurements (mean, standard deviation, maximum, minimum, 25, 50, and 75 percentiles) is extracted from the instantaneous amplitude estimates [11]. These values are calculated on the segmented vasculature inside the R2 region. Since the range of vessel diameters in the images is between 3 and 30 pixels, the analysis focuses on medium, low, very-low and ultra-low frequencies. By combining these scales in six different ways, 42 features for the classifier are obtained.

J. Classification

A partial least squares (PLS) [12] classifier is used to identify images with HR. This regression classifier is a robust method that works well when the predictor variables are highly correlated. A total of 49 features are input to the classifier as the independent variables. The dependent variable is the clinical determination of HR or normal from the optometrist. The output of the classifier is a floating point prediction of the presence of HR in each image. Sensitivity and specificity are obtained by applying a threshold to the output of the classifier. The classifier was validated using leave-one-out case cross validation.

IV. Results

A. Artery-Vein classification

Figure 5 shows the results of the artery vein classification. A total of 1048 segments of vessels for the 74 images were analyzed in the R1 region. The cross validation resulted in average AUC of 0.94. An operating point in the ROC curve of 88.5% and 85.7% for sensitivity and specificity, respectively, was selected. This operating point resulted in a classification accuracy of 87%.

B. Artery-Vein ratio

Fig. 6 shows the boxplots of calculated AVR for the two classes: normal and HR. The median for the normal class was 0.67 and the median for the hypertension class was 0.58.

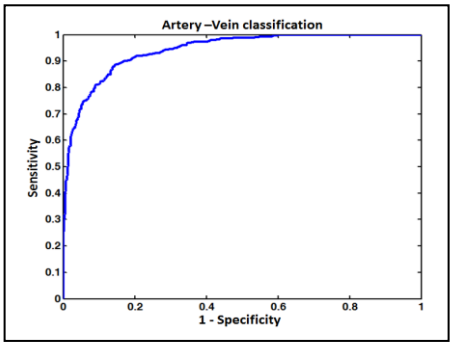

Figure 5. ROC curve of the classification of arteries and veins.

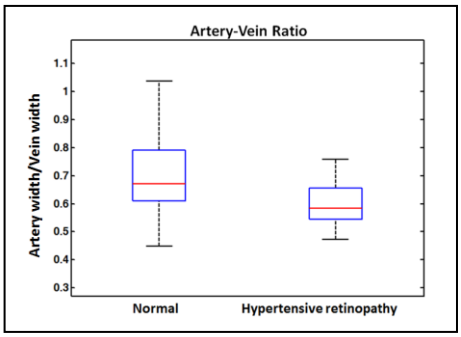

Figure 6. Boxplots of the AVR for the normal and HR subjects.

C. Silver/copper wiring

Two sample t-tests were used to reject the null hypothesis, which assumes that the features used to characterize silver/copper wiring are equally distributed on both HR and normal subjects. We obtain p-values of 0.0433 for red and 0.0045 for saturation channels, so we can infer that both measurements are helpful to discriminate HR and normal subjects.

D. Tortuosity index

Figure 7 shows the tortuosity indices using method 2. The same trend is observed for the other two methods specified in the previous section. Two sample t-tests were also applied in this case, obtaining p-values of 0.0088, 0.0077 and 0.0350 for methods 1, 2 and 3 respectively. Therefore, we reject the hypothesis that both categories have the same tortuosity distribution.

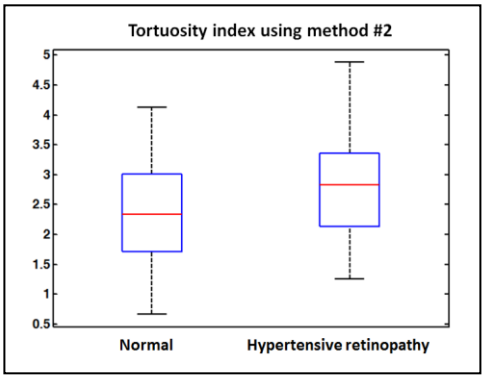

Figure 7. Boxplots of the tortuosity index using the method #2 for the normal and HR subjects.

E. *Hypertension classification*

Fig. 8 shows the ROC curve for the classification of HR. An AUC of 0.84 is obtained with best sensitivity/specificity of 90%/67%. The maximum accuracy is 80%.

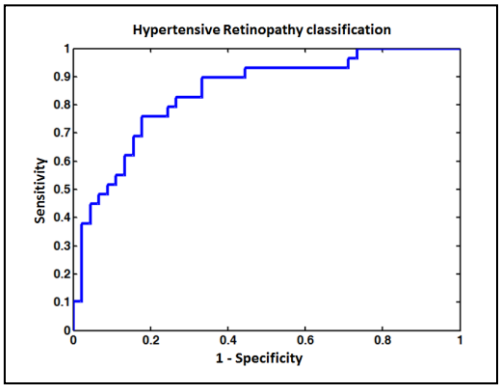

Figure 8. ROC curve for the classification of HR.

V. Discussion and Conclusions

Our results for mean AVR in normal subjects are comparable with the results presented by Knutdson et al. [5], which used a semi-automatic computer software for vessel measurements (mean AVR = 0.69); and Niemeijer et al. [13], which used a fully automatic system in 40 images (mean AVR 0.67). Since the width of the arteries for HR subjects is smaller, a lower mean value as the obtained in this approach was expected (mean AVR = 0.58). However, this cannot be compared with other publications since it depends on the degree of the disease.

The features obtained for detecting copper/silver wiring (especially the red channel) present small differences between classes (p-value = 0.0433). One of the reasons of this is that not all the HR subjects present these changes in the vasculature. In addition, our results may be negatively affected since we only analyzed the R1 region, although changes in the arteries could also be found in the R2. Therefore, we plan to include the R2 region in the future.

We present a fully automatic methodology for detecting HR in digital fundus images. This methodology is based on characterization of retinal vessel features and linear regression classification.

Computational image features of tortuosity, texture, color, and AVR are used as inputs to a linear regression classifier that achieves 80% accuracy in detecting HR.

Our methodology was tested on 74 images which may not be representative of the population distribution in terms of age, gender, and fundus pigmentation. Therefore, we are currently in the process of validating our methodology on an augmented set of images that includes groups with more representative demographic data.

Although the extracted features are informative for the detection of HR, they are not absolutely conclusive for diagnosis on all cases. To obtain a better performance, we are working in methods to determine AV nicking, branching angle, and emboli plaque as a means to cover the spectrum of vascular changes due to HR.

Acknowledgment

The authors thank the Retina Institute of South Texas (RIST) for providing data for this research. This work was supported in part by NEI grants R44EY020015, R43EY024169.

References

[1] T. Y. Wong, R. Klein, A.R. Sharrett, et al. "Retinal arteriolar diameter and risk for hypertension," *Ann. Intern. Med*., vol. 140, pp. 248–255, 2004.

[2] T. Y. Wong, R. Klein, F.J. Nieto, et al. "Retinal microvascular abnormalities and 10-year cardiovascular mortality: a population-based case-control study", *Ophthalmology*, vol. 110, pp. 933–940, 2003.

[3] T. Y. Wong, R. Klein, et al., "Hypertensive Retinopathy and Risk of Stroke", *published online in Hypertension* 2013.

[4] H Yu, E S Barriga, C Agurto, S Echegaray, M S Pattichis, W Bauman, and P Soliz, "Fast Localization and Segmentation of Optic Disc in Retinal Images using Directional Matched Filtering and Level Sets", *Information Technology in Biomedicine, IEEE Transactions on*, vol. 16 no 4, pp. 644-657, 2012.

[5] M. D. Knudtson, K. E. Lee, L. D. Hubbard, T. Y. Wong, R. Klein, and B. E. K. Klein, "Revised formulas for summarizing retinal vessel diameters," *Current Eye Research*, vol. 27, no. 3, pp. 143–149, 2003

[6] H. Yu, S. Barriga, C. Agurto, G. Zamora, W. Bauman and P. Soliz, "Fast Vessel Segmentation in Retinal Images Using Multiscale Enhancement and Second-order Local Entropy", *Proc. SPIE Medical Imaging 8315*, 2012.

[7] Rafael C. Gonzales, Richard E. Woods, Digital Image Processing, second edition, Prentice Hall, 2002.

[8] H. Yu, S. Barriga, C. Agurto and P. Soliz, "Automated Retinal Vessel Type Classification in Color Fundus Images", *Proc. SPIE Medical Imaging 8670,* 2013

[9] R. Turior and Uyyanonvara, "Curvature-based tortuosity evaluation for Infant Retinal Images," *Journal of Information Engineering and Applications*, vol. 2, no. 8, 2012.

[10] Joshi V, Reinhardt JM, Abramoff MD, "Automated measurement of retinal blood vessel tortuosity", *SPIE Med. Imag.*, vol. 7624, 2010.

[11] C Agurto, H Yu, V Murray, et al., " Detection of Neovascularization in the Optic Disc Using An AM-FM Representation, Granulometry, and Vessel Segmentation*", 34th IEEE EMBS*, 2012.

[12] de Jong, S. "SIMPLS: An Alternative Approach to Partial Least Squares Regression." *Chemometrics and Intelligent Laboratory Systems.* vol. 18, 1993, pp. 251–263.

[13] M. Niemeijer, X. Xu, A.V. Dumitrescu, et al. "Automated Measurement of the Arteriolar-to-Venular Width Ratio in Digital Color Fundus Photographs". *Transactions on Medical Imaging*, vol. 30, no. 11, pp. 1941-1950, 2011.